arXiv:1606.07016v1 [hep-ph] 22 Jun 2016

Modelling the nuclear parton distributions

S A Kulagin

Institute for Nuclear Research of the Russian Academy of Sciences, Moscow 117312, Russia

E-mail: sergey.kulagin@gmail.com

Abstract. We review a semi-microscopic model of nuclear parton distributions, which takes into account a number of nuclear effects including Fermi motion and nuclear binding, nuclear meson-exchange currents and off-shell corrections to bound nucleon distributions as well as nuclear shadowing effect. We also discuss applications of the model to the lepton-nuclear deep-inelastic scattering, Drell-Yan process and neutrino total cross sections.

1. Introduction

The leading contribution to cross sections of various hard processes is determined by the parton distributions (PDFs). Thus, PDFs are universal process-independent characteristics of the target at high invariant momentum transfer Q. The nuclear parton distributions (NPDFs) are the subject of significant nuclear effects which span a wide region of Bjorken x as demonstrated by the deep inelastic scattering (DIS) experiments and the measurements of the Drell-Yan process (DY) (for a review see [1, 2]). A relative rate of nuclear effects is more than one order of magnitude larger than the ratio of the nuclear binding energy to the nucleon mass thus indicating that the nuclear environment plays an important role even at high energies and momenta.

A number of phenomenological approaches to NPDFs are available in literature [3, 4, 5, 6]. Although such studies are useful in constraining nuclear effects for different partons, they provide little information about the underlying physics responsible for the nuclear corrections. In this contribution we follow a different approach and present the results of a study of NPDFs using a model of Ref.[7] which takes into account a few different mechanisms of nuclear corrections. The model, which is briefly reviewed in Sec.2, explains the observed x, Q^2 and A dependencies of the nuclear structure functions in the deep inelastic scattering (DIS) for a wide range of nuclear targets from ^{2}H to ^{207}Pb [7, 8, 9]. In what follows we focus on the region of high Q^2 and review predictions [10] of nuclear effects for the valence and sea quark distributions (Sec.2), discuss applications to nuclear DIS, nuclear DY process (Sec.3) and the total neutrino-nuclear cross sections (Sec.4).

2. Nuclear PDFs and DIS

We will use the notation $q_{a/T}(x,Q^2)$ for the distribution of quarks of the flavor a in a target T. The parton distributions in a nucleus receive a number of contributions and can be summarized as [7, 10]

$$q_{a/A} = \Big\langle q_{a/p} \Big\rangle + \Big\langle q_{a/n} \Big\rangle + \delta q_a^{\rm coh} + \delta q_a^{\rm MEC}. \qquad (1)$$

For brevity, we suppress explicit dependencies on x and Q^2 in Eq.(1). The first two terms on the right side are the contribution from the partons from bound protons and neutrons. The

brackets stand for the averaging with the energy-momentum distribution of bound nucleons in a nucleus, as discussed in detail in Ref.[7, 10]. Note that the evaluation of these terms requires the proton and the neutron PDFs in off-mass shell region [11]. The off-shell correction together with the nucleon momentum distribution (Fermi motion) and the nuclear binding effect [12] plays an important role in the valence quark region [7, 9].

The correction $\delta q^{\rm coh}$ arises due to propagation effects of intermediate hadronic states of a virtual boson in nuclear environment. This term involves contributions from multiple scattering series and typically lead to a negative correction relevant at low x (nuclear shadowing effect, for a review see, e.g., Ref.[14]).

The last term in Eq.(1) is a contribution from the meson degrees of freedom in nuclei. We recall that the meson fields mediate the nucleon-nucleon interaction in nuclei and also generate an additional quark-gluon content in nuclei. This term is relevant for intermediate region of x and results in a some enhancement of the nuclear sea quark distribution. Also its contribution is important to balance the overall nuclear light-cone momentum. More details on the treatment of each term in Eq.(1) can be found in Refs.[7, 10].

In analysis of Ref.[10] we choose the PDFs with definite C-parity $q^{\pm} = q \pm \bar{q}$ as a basis. Note that the C-even combination xq^{+} contributes to the structure function F_2, for both the charged-lepton and neutrino deep-inelastic scattering, while the C-odd xq^{-} is the valence quark distribution which contributes to the neutrino structure function xF_3. For light quarks we also consider the isoscalar $q_0 = u+d$ and the isovector $q_1 = u-d$ combinations. Below we summarize our results on the nuclear valence and sea quark PDFs.

In order to illustrate the nuclear effects, in Fig.1 we show the ratios $R_a^A = q_{a/A}/(Zq_{a/p} + Nq_{a/n})$ calculated for the valence quarks (left panel) and the antiquarks (right panel) in the lead nucleus. Here Z and N are the proton and the neutron number in the discussed nucleus with the total nucleon number $A = Z + N$, and $q_{a/p}$ and $q_{a/n}$ are the free proton and the neutron PDF, respectively. As can be seen from Fig.1 the resulting nuclear effect is different for the

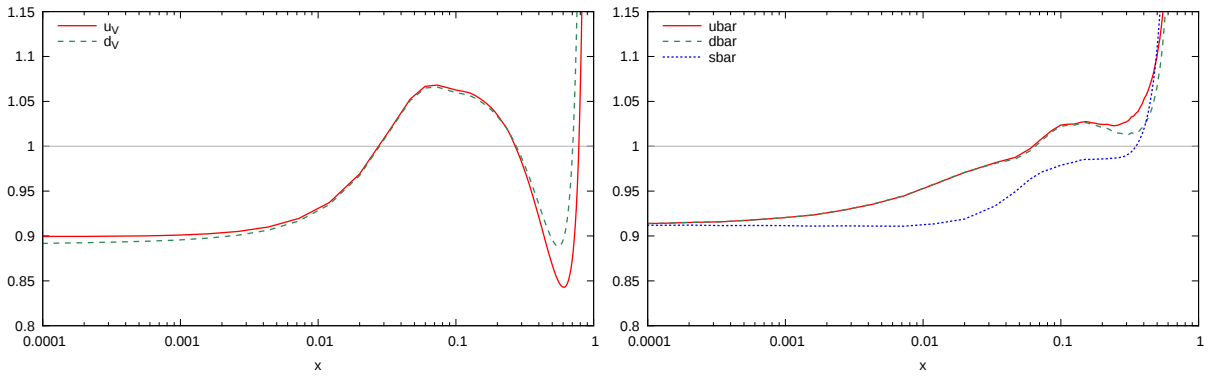

Figure 1. The nuclear ratios for the valence quarks (left panel) and the $\bar{u}$, $\bar{d}$, and $\bar{s}$ antiquarks (right panel) in ^{208}Pb calculated at $Q^2 = 25\,\mathrm{GeV}^2$ (see text for more detail).

nuclear valence and sea distribution and also depends on the PDF flavor. We briefly comment on characteristic features of the nuclear ratios for different PDFs, for a more detail discussion see Ref.[10].

In the region $x \ll 0.1$, all NPDFs are suppressed due to the nuclear *shadowing* effect (a negative $\delta q^{\rm coh}$ term). Note that the rate of this effect is not universal and differs for the valence and sea quark distribution [7, 10]. We also remark that the result of averaging of the nucleon PDF with the nuclear spectral function in the first two terms in the right side of Eq.(1) depends on the details of the x dependence of considered PDF. For this reason, this correction is positive

for the valence quarks thus partially reducing the shadowing effect. For the sea quarks this correction is negative in this region. However, the MEC correction is positive and we also have a partial cancellation of different effects.

In the intermediate region of $x \sim 0.1$ (which is usually referred to as *antishadowing* region) we observe interplay between different nuclear corrections. For the valence quark PDF (C-odd q^- distribution) we find an enhancement which is due to constructive interference in the multiple scattering effect between the C-even and C-odd amplitudes in the $\delta q^{\rm coh}$ term. The antishadowing effect on the antiquark PDFs is somewhat weaker and shifted towards larger x because of a partial cancellation between different contributions [10].

At large $x > 0.2$ the nuclear PDFs are dominated by incoherent scattering from bound nucleons, i.e. by the first term on the right in Eq.(1). For the valence quarks, the averaging of the proton and neutron PDFs with the nuclear spectral function together with the off-shell correction produces a pronounced 'EMC-effect' shape at large x [7]. This effect was noticed long ago in [12, 13] and further discussed in Ref.[7]. The relative rate of this correction strongly depends on the particular x dependence of the given PDF and for this reason the ratios $R_{\rm val}$ and $R_{\rm sea}$ are quite different at large x.

It should be remarked that different nuclear effects are related through a number of sum rules which reflect different global symmetries. In particular, the conservation of the valence quark number links together the off-shell and the shadowing corrections to the valence quark distributions. In Ref.[7, 10] the normalization conditions for the isoscalar and the isovector valence quark distributions were used as equations to determine the unknown amplitudes controlling the coherent nuclear correction. We then solved these equations in terms of the off-shell correction to the corresponding distributions. The energy-momentum conservation causes the light-cone momentum sum rule at two different levels. At the hadronic level, the nuclear light-cone momentum is shared between nucleons and mesons. This requirement allows to constrain the MEC correction to NPDFs. At the partonic level, the light-cone momentum is balanced between quarks, antiquarks and gluons. The study of different contributions to the light-cone momentum sum rule can provide insights on modification of gluon distribution in nuclei.

A detailed analysis of data on the ratio of the DIS structure functions for different nuclear targets $R_2(A'/A) = F_2^{A'}/F_2^A$ (usually the ratio is taken with respect to the deuteron) with targets ranging from ^{4}He to ^{208}Pb shows a very good agreement of model predictions with observed x, Q^2 and nuclear dependence of data [7, 9]. The performance of discussed model is illustrated in Fig.2, in which we show the model predictions in comparison with data for a number of nuclei. However, it should be remarked that the model predictions in Fig.2 are given at a fixed $Q^2 = 5\,{\rm GeV}^2$ while the data from different measurements have essentially different average Q^2. Furthermore, each x bin of data has different average Q^2 value. For a detailed comparison with data and discussion of consistency of different data sets see Ref.[7, 9].

3. NPDFs and Drell-Yan process

The reaction of muon pair production in hadron-hadron collisions (Drell-Yan process) is an important source of information on the proton, pion and nuclear PDFs [20]. In the context of NPDFs, the use of DY data in combination with DIS data allows a separation of the nuclear valence and sea quark distributions. In the DY reaction with the proton beam by tuning the kinematics of the muon pair one can select a region in which the DY cross sections are driven by annihilation of valence quarks in the beam and antiquarks in the target. Then the ratio of the DY cross sections off different nuclear targets provide a tool to measure the nuclear dependence of antiquark PDFs

$$\frac{\sigma_A^{DY}}{\sigma_B^{DY}} \approx \frac{\bar{u}_A(x_T) + \bar{d}_A(x_T)}{\bar{u}_B(x_T) + \bar{d}_B(x_T)}, \qquad (2)$$

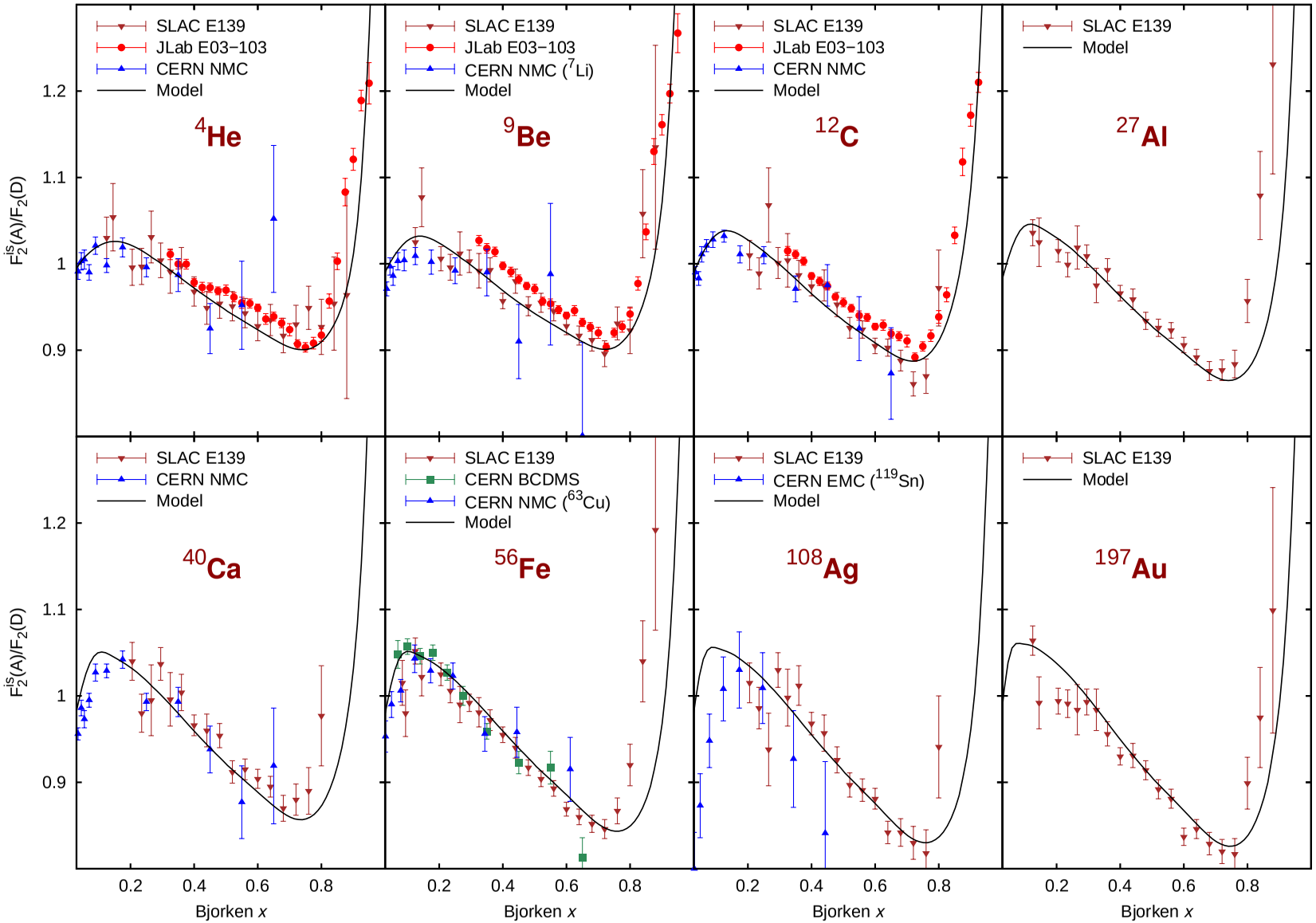

Figure 2. The ratio of a nucleus to the deuteron structure function F_2^A/F_2^D for different nuclei. Data are from experiments at CERN (EMC [15], NMC [16] and BCDMC [17]), SLAC (E139 [18]), and JLab [19]. The model predictions are given for a fixed $Q^2 = 5\,\mathrm{GeV}^2$.

where x_T is the Bjorken variable for a nuclear target. This ratio was measured in the experiments E772 [21] and E866 [22] with the proton beam momentum 800 GeV/c at Fermilab in the region $x_T < 0.15$ for a number of nuclear targets. In contrast to DIS, the DY data show no *antishadowing* (i.e. enhancement of nuclear antiquark distributions) at $x_T \sim 0.1$ that was a long standing puzzle since the nuclear binding should result in an excess of nuclear mesons, which is expected to produce a marked enhancement in the nuclear anti-quark distributions [25].

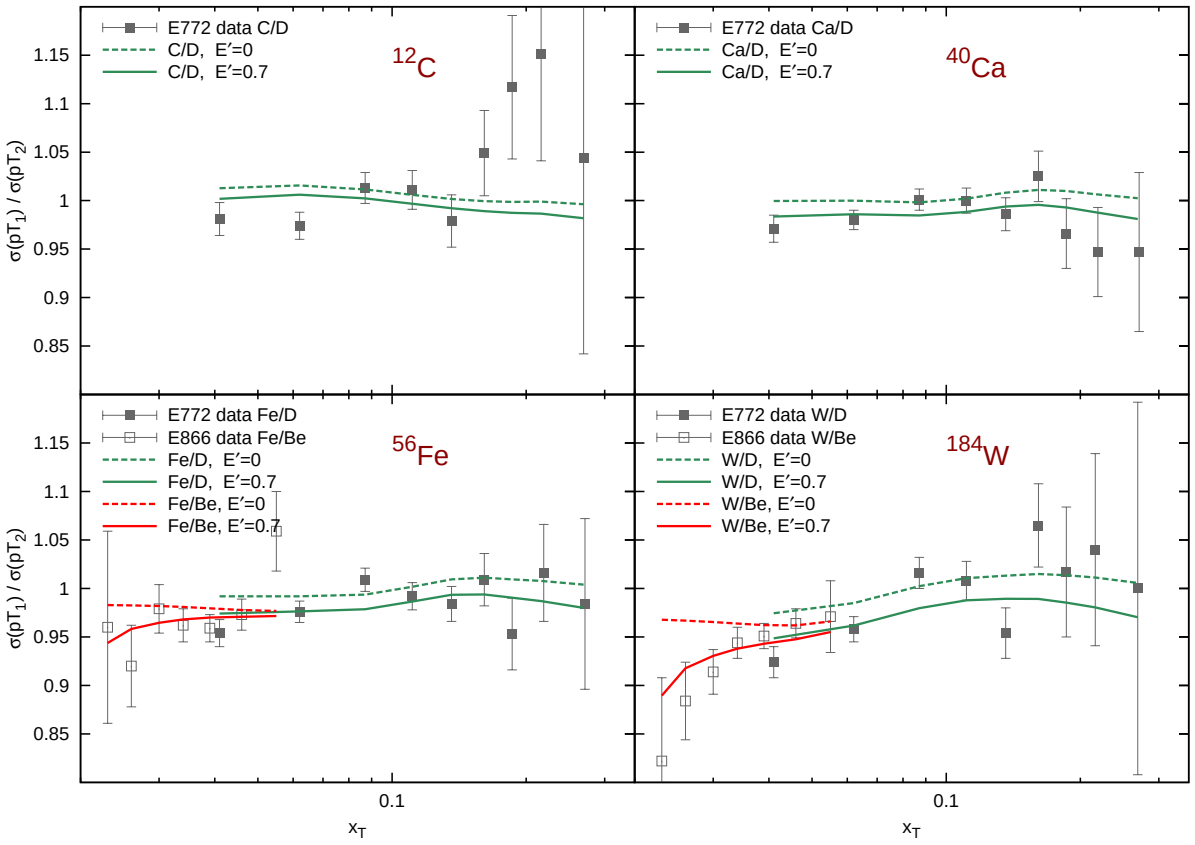

Figure 3. Ratio of the DY reaction cross sections for different nuclei vs. x_T. Data points are from the E772 experiment [21] (■) and E866 experiment [22] (□). Note that the ratio is normalized to one bound nucleon and taken relative to the deuteron for E772 and ^{9}Be for E866. The curves are the predictions of Ref.[10] for the deuteron (green) and beryllium (red) ratios with (——) and without (- - - -) the projectile energy loss effect (see text and legend).

As discussed above, the model of Ref.[7, 10] predicts a significant cancellation of different nuclear effects in the antiquark distribution in the region $x \sim 0.1$ in agreement with the nuclear DY data. In Fig.3 we show the data along with our predictions on the ratios of the DY cross sections [10]. We also remark that nuclear dependence of the DY process comes from two different sources: (i) the modification of the nuclear target PDFs, and (ii) the initial state interaction of the projectile particle (parton) within the nuclear environment that causes the parton energy loss [23] before annihilation into a dimuon pair. The rate of this effect is characterized by the parton energy loss in a nucleus per unit length E' and effectively results in a change of the projectile parton Bjorken x [24] which in turn modify the ratio in Eq.(2).

The data from the E866 experiment is shifted towards lower values of target's x_T and higher values of projectile's x_B with respect to E772 data thus falling into a region where both the

shadowing and the energy loss effects become more prominent. Our analysis [10] indicates that the model of Ref.[7] is in a good agreement with data at a moderate energy loss effect. The solid curves in Fig.3 show our predictions with $E' = 0.7$ GeV/fm. Note also that the cross section ratios are taken relative to the deuterium for E772 and beryllium for E866. For this reason the corresponding curves in Fig.3 are not identical in the overlap region.

4. NPDFs and total neutrino cross sections

For the reason of statistics the neutrino scattering data have been collected on heavy nuclei. Thus the comparison of theory predictions with data on the neutrino cross sections serves as an important and independent test of both the proton and the nuclear PDFs. In the following we focus on the total cross sections as the available data on total cross sections have typically better accuracy than the corresponding measurements of differential cross sections and span a wide energy region.

We calculate the total cross sections by integrating the double differential inelastic cross sections $\mathrm{d}^2\sigma^{(\nu,\bar{\nu})}/\mathrm{d}x\mathrm{d}y$ over allowed region of x and y. In the leading α_S order we have for the total cross sections off an isoscalar target (i.e. the combination of $p+n$ or a nucleus with equal number of protons and neutrons)

$$\frac{\sigma_{\rm tot}(E)}{E} = \frac{2G_F^2 M}{3\pi(1+Q^2/M_W^2)^2}\left(x_0^+ \pm x_0^-/2 + 3x_s\right), \tag{3}$$

where G_F is the Fermi coupling constant, M and M_W are the proton and the W-boson mass, $x_0^\pm = \int_0^1 \mathrm{d}x x q_0^\pm(x,Q^2)$ is the average light-cone momentum for the isoscalar C-even (q_0^+) and C-odd (q_0^-) quark distributions, and, similarly, x_s is the light-cone momentum carried by s quark (we assume $s=\bar{s}$ and also neglect a small contributions from heavy quarks). The $+/-$ sign in Eq.(3) corresponds to $\nu/\bar{\nu}$ scattering. The average invariant momentum transfer Q in Eq.(3), although difficult to evaluate precisely, by order of magnitude $Q^2 = ME/2$.

In Fig.4 we show the results on the total cross section for the isoscalar nucleon calculated by Eq.(3). We also go beyond the LO approximation and numerically compute the (anti)neutrino cross sections using the NNLO structure functions with the NNLO PDFs of Ref.[29].

A few comments are in order. The ratio $\sigma_{\rm tot}(E)/E$ is almost a constant in the considered energy region. A weak energy dependence comes through Q^2 dependence of W-boson propagator and the parton distributions (structure functions). A higher order α_S corrections on the structure functions result in a overall negative correction to the total cross section reducing significantly the LO cross section in the energy region up to a few hundred GeV. It is worth noting that this effect leads to a better agreement with data.

In Fig.4 we show the data from CCFR [26], NOMAD [27] and MINOS [28] neutrino experiments. Note, however, those data were taken on different nuclear targets, ^{56}Fe for CCFR and MINOS and ^{12}C for NOMAD. Therefore, in order to make a meaningful comparison, it is important to address the nuclear dependence of the (anti)neutrino cross sections. For this reason we discuss the normalized ratios of the nuclear and the proton and neutron neutrino cross sections $R_A^\nu = \sigma_A^\nu/(Z\sigma_p^\nu + N\sigma_n^\nu)$ and a similar ratio $R_A^{\bar{\nu}}$ for antineutrino. In Fig.5 (left panel) we show the ratios R_A^ν and $R_A^{\bar{\nu}}$ calculated for ^{12}C and ^{56}Fe nuclei using the NNLO structure functions of Ref.[29] within the approach outlined above (for more detail see Refs.[8, 10]). We observe that in considered energy region the rate of nuclear effects is about 2% at maximum for both the neutrino and the antineutrino and gradually decreasing with energy. Note also that the ratios R_A^ν and $R_A^{\bar{\nu}}$ show almost no nuclear dependence that justifies the comparison of total neutrino cross sections for different nuclear targets in Fig.4.

Figure 5 indicates a suppression of the neutrino-nuclear total cross section while the antineutrino cross section is somewhat enhanced in nuclei (the latter in turn further improves

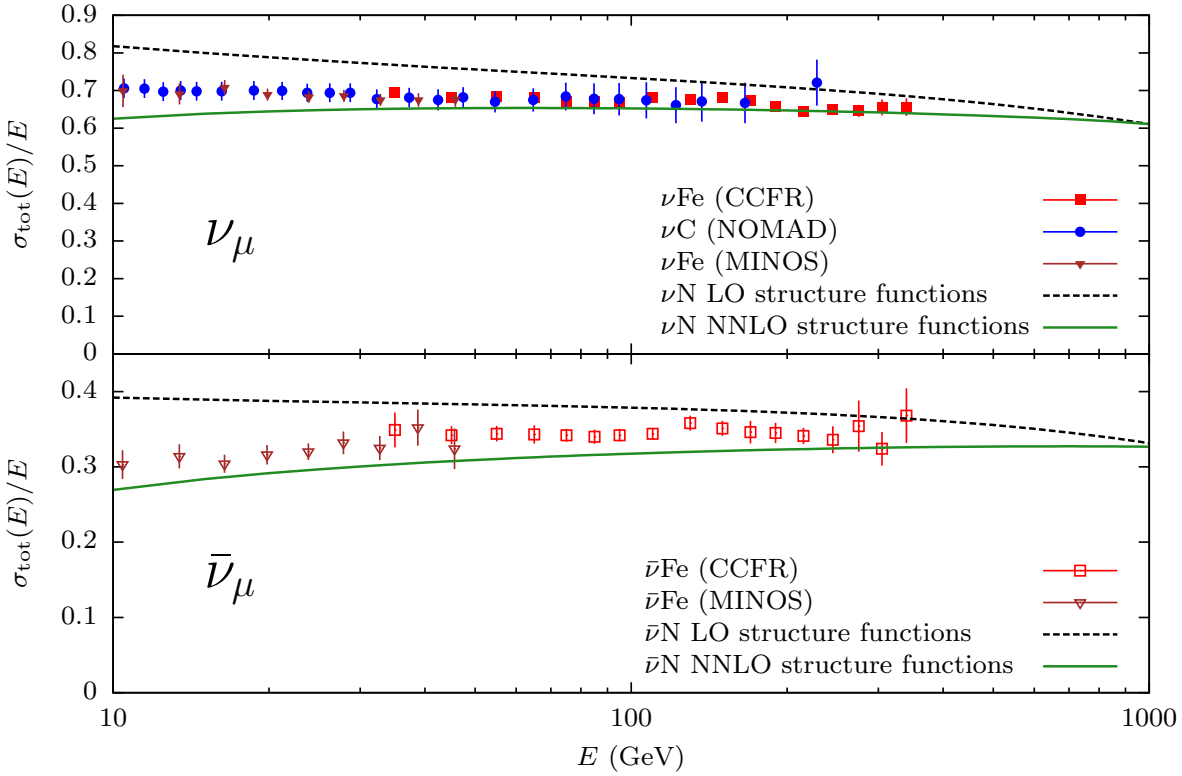

Figure 4. The neutrino (upper panel) and antineutrino (lower panel) total cross sections as a function of neutrino energy E. The units are $10^{-38}\,\mathrm{cm}^2/\mathrm{GeV}$. The data points are the cross sections per one bound nucleon from CCFR [26], NOMAD [27] and MINOS [28] experiments corrected for the neutron excess in iron. The curves are the LO (dashed) and the NNLO (full) predictions for the isoscalar nucleon calculated with the PDFs of Ref.[29].

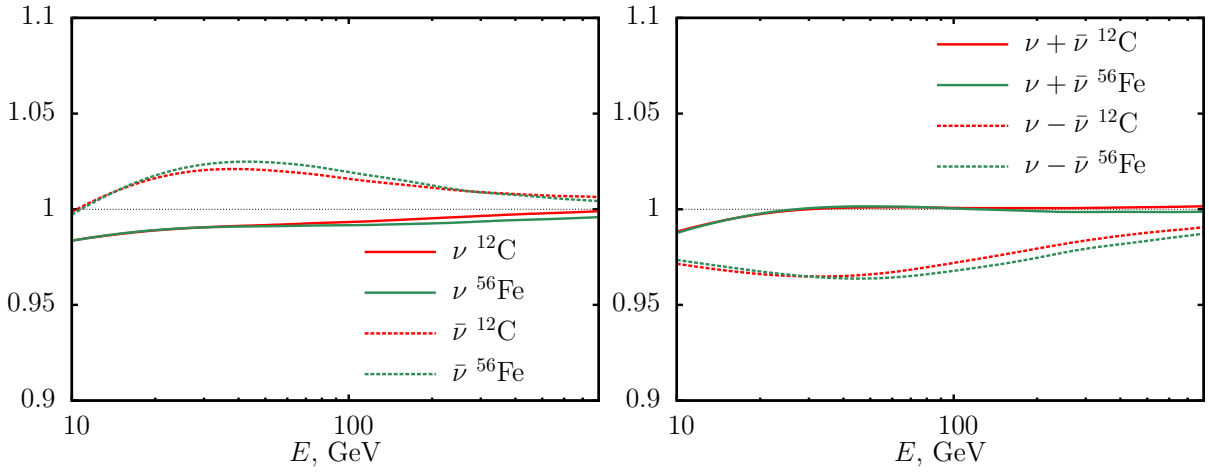

Figure 5. Left panel: The ratios R_A^ν (solid curve) and $R_A^{\bar{\nu}}$ (dashed curve) calculated for ^{12}C (red) and ^{56}Fe (green) nuclei as a function of neutrino energy E. Right panel: Similar ratios for the C-even $\nu+\bar{\nu}$ (solid) and C-odd $\nu-\bar{\nu}$ (dashed) combinations of the total cross sections.

agreement with $\bar{\nu}$ data in Fig.4). These two effects cancel each other for the C-even combination $\nu+\bar{\nu}$ of the cross sections as illustrated in the right panel of Fig.5. On the other hand, the nuclear correction to the C-odd combination $\nu-\bar{\nu}$ is somewhat enhanced.

It is instructive to compare the nuclear corrections for the total cross sections with those for PDFs (see Fig.1 and 2). We note in this context a direct relation between the total neutrino

cross sections and average light-cone momenta of different quark PDFs in Eq.(3). The nuclear modification of average light-cone momenta have much smaller magnitude compared to a typical amplitude of nuclear effects for PDFs shown in Fig.1 and 2. This is because of a cancellation between nuclear corrections of different sign in different kinematic regions in the integral over the Bjorken x. The isoscalar $\nu+\bar{\nu}$ combination of the total cross sections is proportional to the total quark and antiquark light-cone momentum in the target. Thus a cancellation of nuclear effects in $\sigma(\nu+\bar{\nu})$ suggests that the overall light-cone momentum of quarks and antiquarks does not change in nuclei. Referring to the light-cone sum rule we also conclude that the average gluon light-cone momentum is not modified in nuclei. However, discussion of associated problems goes beyond of the scope of the present article and will be given elsewhere.

5. Summary

In summary, we reviewed a semi-microscopic model of nuclear PDFs addressing a few different mechanisms of modification of PDFs in nuclear environment. A number of applications were discussed including charged-lepton DIS, proton-nuclear DY reaction and calculation of total (anti)neutrino-nuclear cross sections in charged-current interaction.

I thank R. Petti for fruitful collaboration on the topics of this paper and A. Kataev for motivating discussions. I am grateful to the Organizing Committee of ACAT 2016 Workshop for support and for creating a friendly and working environment during the meeting.

The work was supported by the Russian Science Foundation grant No. 14-22-00161.

References

[1] Arneodo M 1994 *Phys. Rept.* **240** 301 (1994)
[2] Norton P R 2003 *Rept. Prog. Phys.* **66** 1253 (2003)
[3] Eskola K J, Paukkunen H and Salgado C A 2009 *J. High Energy Phys.* JHEP0904(2009)065
[4] Hirai M, Kumano S and Nagai T-H 2007 *Phys. Rev.* C **76** 065207 (2007)
[5] de Florian D, Sassot R, Zurita P and Stratmann M 2012 *Phys. Rev.* D **85** 074028 (2012)
[6] Kovarik K *et al.* 2015 *Preprint* arXiv:1509.00792 [hep-ph].
[7] Kulagin S A and Petti R 2006 *Nucl. Phys.* A **765** 126 (2006)
[8] Kulagin S A and Petti R 2007 *Phys. Rev.* D **76** 094023 (2007)
[9] Kulagin S A and Petti R 2010 *Phys. Rev.* C **82** 054614 (2010)
[10] Kulagin S A and Petti R 2014 *Phys. Rev.* C **90** 045204 (2014)
[11] Kulagin S A, Piller G and Weise W 1994, *Phys. Rev.* C **50** 1154 (1994)
[12] Akulinichev S V, Kulagin S A and Vagradov G M 1985, *Phys. Lett.* B **158** (1985) 485
[13] Kulagin S A 1989, *Nucl. Phys.* A **500** 653 (1989)
[14] Piller G and Weise W 2000, *Phys. Rept.* **330** 1 (2000)
[15] Ashman J *et al.* 1993, *Z. Phys.* C **57** 211 (1993)
[16] Armeodo M *et al.* 1995, *Nucl. Phys.* B **441** 12 (1995); *Ibid.* 3 (1995)
[17] Bari G *et al.* 1985, *Phys. Lett.* B **163** 282 (1985)
[18] Gomez J *et al.* 1994, *Phys. Rev.* D **49** 4348 (1994)
[19] Seely J *et al.* 2009, *Phys. Rev. Lett.* **103** 202301 (2009)
[20] Peng J C and Qiu J W 2014, *Prog. Part. Nucl. Phys.* **76** 43 (2014)
[21] Alde D M *et al.* 1990, *Phys. Rev. Lett.* **64** 2479 (1990).
[22] Vasilev M A *et al.* 1999, *Phys. Rev. Lett.* **83** 2304 (1999).
[23] Bjorken J D 1982, FERMILAB-PUB-82-059-THY
[24] Garvey G T and Peng J C 2003, *Phys. Rev. Lett.* **90** 092302 (2003)
[25] Bickerstaff R P, Birse M C and Miller G A 1984, *Phys. Rev. Lett.* **53** 2532 (1984)
[26] Seligman W G 1997, FERMILAB-THESIS-1997-21
[27] Wu Q *et al.* 2008, *Phys. Lett.* B **660** 19 (2008)
[28] Adamson P *et al.* 2010, *Phys. Rev.* D **81** (2010) 072002
[29] Alekhin S, Blumlein J, and Moch S 2014, *Phys. Rev.* D **89** 054028 (2014)